

Estimating Salinity Variance Dissipation Rate from Conductivity Microstructure Measurements

JONATHAN D. NASH AND JAMES N. MOUM

College of Oceanic and Atmospheric Sciences, Oregon State University, Corvallis, Oregon

(Manuscript received 16 July 1997, in final form 13 April 1998)

ABSTRACT

At the smallest length scales, conductivity measurements include a contribution from salinity fluctuations in the inertial-convective and viscous-diffusive ranges of the turbulent scalar variance spectrum. Interpreting these measurements is complicated because conductivity is a compound quantity of both temperature and salinity. Accurate estimates of the dissipation rate of salinity variance χ_s and temperature variance χ_T from conductivity gradient spectra $\Psi_{c_i}(k)$ require an understanding of the temperature-salinity gradient cross spectrum $\Psi_{s,T_i}(k)$, which is bounded by $|\Psi_{s,T_i}| \leq \sqrt{\Psi_{s_i}\Psi_{T_i}}$.

Highly resolved conductivity measurements were made using a four-point conductivity probe mounted on the loosely tethered vertical profiler *Chameleon* during cruises in 1991 and 1992. Thirty-eight turbulent patches were selected for homogeneity in shear, temperature gradient, and salinity gradient fluctuations and for clear relationship between temperature and salinity. Estimates of χ_T and χ_s from the conductivity probe are found to agree with independent estimators from a conventional thermistor probe.

1. Introduction

Many important inferences have been made from measurements of temperature microstructure during the past 30 years (Gregg 1987). Measurement of salinity microstructure is much more difficult because it requires resolving much smaller scales. In addition, coincident measurements of temperature (T) and conductivity (C) are required to determine salinity (S). Using present sensor technology, it is impossible to coincidentally resolve C and T at the submillimeter scales required to observe the smallest-scale fluctuations of a turbulent flow field. Fully resolved measurements of this type would allow direct calculation of the salinity spectrum, χ_s , and vertical salt fluxes, for example.

One motivation for this work is the determination of the turbulent diffusivity for salt, K_s . In regions in which salinity gradients are important to the stratification, K_s is required to characterize the flux of buoyancy $\langle w\rho \rangle$, a dynamically important quantity. For lack of any better estimator (such as that supported by experimental data), K_s has been assumed to be numerically equal to K_T , the turbulent diffusivity for heat, although there is no sound experimental evidence to support this and K_s and K_T are in fact defined differently.

In determining the vertical eddy diffusivity K_θ for a scalar θ , we follow the approach of Osborn and Cox (1972). By neglecting horizontal processes and assuming steady and homogeneous turbulence, the evolution equation for $\langle \theta^2 \rangle$ reduces to

$$\langle w\theta \rangle \left\langle \frac{\partial \theta}{\partial z} \right\rangle = -D_\theta \langle (\nabla \theta)^2 \rangle, \quad (1)$$

where D_θ is the molecular diffusivity of the scalar. The eddy flux $\langle w\theta \rangle$ can be expressed in terms of K_θ as

$$\langle w\theta \rangle = K_\theta \left\langle \frac{\partial \theta}{\partial z} \right\rangle, \quad (2)$$

which requires

$$K_\theta = D_\theta \frac{\langle (\partial \theta / \partial z)^2 \rangle}{\langle \partial \theta / \partial z \rangle^2}. \quad (3)$$

In such a description, scalar fluctuations are indicators of turbulent transport since they are the result of turbulent overturns acting on the mean vertical gradient of θ .

For seawater, the large Schmidt number ($Sc \equiv D_T / D_s \sim 100$) would suggest that eddy diffusivities (at least on some scales) should be very different. For example, it is well known that salt is more effectively transported by salt fingering than heat (Schmitt 1979). In contrast, double-diffusive layering allows heat to be transported much more effectively than salt (Turner 1965). Such physical processes may affect the ratio of eddy diffu-

Corresponding author address: James Moum, College of Oceanic and Atmospheric Sciences, Oregon State University, 104 Oceanography Administration Building, Corvallis, OR 97331-5503.
E-mail: moum@oce.orst.edu

sivities $d = K_S/K_T$ by several orders of magnitude, yet these effects are largely unknown.

The implications of varying d were explored by Garrett and Holloway (1992) using a coarse-resolution primitive equation general circulation model. They found that the thermohaline circulation and general T - S properties are highly affected by small changes in d . Direct field measurements of the turbulent fluxes of S in the ocean are thus imperative to a better understanding of larger-scale phenomena.

Highly resolved salinity measurements and spectra have not been made. However, measurements of C include contributions from both T and S . Sufficiently resolved conductivity spectra and proper interpretation of the local T - S relation permit estimation of both temperature and salinity gradient variance.

To date, highly resolved conductivity measurements have primarily been used to infer temperature microstructure (e.g., Schmitt et al. 1988), because thermistor probes have a relatively slow response time. However, it is only recently that the complexity of the conductivity spectrum was revealed by Washburn et al. (1996). They showed that effects from the T - S relation can affect estimates of χ_T from conductivity measurements by a factor of 20. These effects from salinity are clearly important and have been ignored in the past (Schmitt et al. 1988).

Our measurements are made from a loosely tethered vertical profiler outfitted with a high-resolution, four-pole conductivity probe in addition to our regular microstructure sensors (Moum et al. 1995). Conductivity spectra are sufficiently resolved to make estimates of both χ_T and χ_S .

In the following sections, the Batchelor (1959) theoretical form for the scalar gradient spectrum is reviewed. This is then applied to conductivity gradient spectra, and a method is presented that allows the contributions from T and S to be identified from a single spectrum of C . Examples of typical conductivity spectra are presented to illustrate the methodology. Finally, dissipation rates and eddy diffusivities for both T and S are calculated and compared.

2. Scalar spectra in the inertial and viscous subranges

Measurements of oceanic turbulence from loosely tethered vertical profilers may resolve scales of $O(1\text{ m})$ to $O(1\text{ mm})$. For passive scalars such as heat and salt, spectra include components of the inertial-convective, the viscous-convective, and the viscous-diffusive subranges (Tennekes and Lumley 1972), as shown in Fig. 1.

In 1941, Kolmogorov reasoned that viscosity ν could be important only to the turbulent flow field at wavenumbers of $O(k_s)$, where $k_s \equiv (\epsilon/\nu^3)^{1/4}$ and ϵ is the mean dissipation rate of turbulent kinetic energy. At wavenumbers less than approximately 0.1 – $0.2k_s$, the velocity gradient spectrum results from the cascade of energy

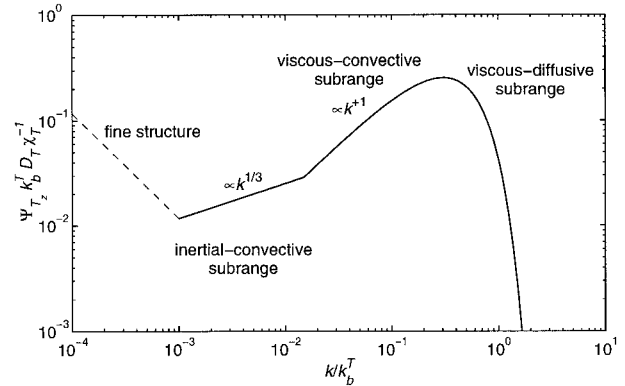


FIG. 1. Three subranges of turbulence in the spectrum of temperature gradient (after Dillon and Caldwell 1980).

from the larger, more energetic scales and is described by

$$\Psi_{u_z}(k) = C_K \epsilon^{2/3} k^{1/3}, \quad (4)$$

where C_K is the Kolmogorov constant. Scalars with molecular diffusivity D_θ much less than ν (described by $\text{Pr} = \nu/D_\theta \gg 1$) are advected passively by turbulent motions in this range. Obukhov (1949) and Corrsin (1951) independently predicted the spectrum of scalar gradient fluctuations Ψ_{θ_z} in the inertial-convective subrange as

$$\Psi_{\theta_z}(k) = C_\theta \epsilon^{-1/3} \chi_\theta k^{1/3}, \quad (5)$$

where

$$\chi_\theta = 6D_\theta \left\langle \left(\frac{\partial \theta}{\partial z} \right)^2 \right\rangle = 6D_\theta \int_0^\infty \Psi_{\theta_z}(k) dk \quad (6)$$

is the mean dissipation rate of scalar variance for isotropic turbulence and C_θ is the Obukhov-Corrsin constant. For high Reynolds number data, $C_\theta \approx 0.4$ (Sreenivasan 1996), although a large range of values have been reported.

At higher wavenumbers, velocity fluctuations are heavily damped by molecular viscosity. In seawater, the molecular diffusivities for heat and salt ($D_T \sim 1.4 \times 10^{-7} \text{ m}^2 \text{ s}^{-1}$, $D_S \sim 1.4 \times 10^{-9} \text{ m}^2 \text{ s}^{-1}$) are both less than viscosity ($\nu \sim 10^{-6} \text{ m}^2 \text{ s}^{-1}$). A consequence is that fluctuations in T and S can exist on smaller scales than fluctuations in velocity.

Without velocity fluctuations to continue the cascade of variance to smaller scales (at which molecular dissipation is effective), Batchelor (1959) suggested that scalar gradients are intensified by strain from turbulent velocity fluctuations at scales k_s^{-1} and larger. The mean least principle strain rate $-\gamma$ (the most negative strain) is responsible for the cascade of variance to higher wavenumbers and is defined by the scaling

$$\gamma \sim (\epsilon/\nu)^{1/2}. \quad (7)$$

A balance between the turbulence-induced strain and molecular diffusion occurs at a wavenumber near

$$(\gamma/D_\theta)^{1/2} \sim \left(\frac{\epsilon}{\nu D_\theta^2}\right)^{1/4} \equiv k_b^\theta. \quad (8)$$

Batchelor (1959) calculated the spectral shape for scalar fluctuations in the viscous ranges. For the range of wavenumbers in which molecular diffusion is not important ($k \ll k_b^\theta$), the spectrum of scalar gradient Ψ_{θ_z} may be written as (Gibson and Schwarz 1963)

$$\Psi_{\theta_z}(k) = \frac{\chi_\theta}{\gamma} k, \quad (9)$$

which is the viscous–convective subrange.

The term D_θ becomes important in the viscous–diffusive subrange (near $k \sim 0.1k_b^\theta$), and the one-dimensional form of the Batchelor spectrum may be written as (Gibson and Schwarz 1963; Dillon and Caldwell 1980)

$$\Psi_{\theta_z}(k) = \frac{(q/2)^{1/2} \chi_\theta}{k_b^\theta D_\theta} f(\alpha)$$

and

$$f(\alpha) = \alpha \left\{ e^{-\alpha^2/2} - \alpha \int_\alpha^\infty e^{-x^2/2} dx \right\}, \quad (10)$$

where $\alpha = (2q)^{1/2} k/k_b^\theta$. Although q [the factor relating γ to ϵ in Eq. (7)] is sometimes considered to be a universal constant, estimates of q vary widely. Dillon and Caldwell (1980) suggested a range from $3\sqrt{2}$ to 5. Batchelor used $q = 2$. Gargett (1985) found that $q = 12$ was required to describe temperature spectra formed from highly isotropic velocity fields. Although not universally accepted as a form for turbulent scalar spectra (e.g., Gargett 1985), we use the Batchelor form as our benchmark for the scalar spectrum. An alternate form of the scalar variance spectrum has been proposed by Kraichnan (1968). The question of whether these universal forms appropriately describe the gradient spectra of either T or S will be addressed in future work.

Gibson and Schwarz (1963) first provided experimental evidence of the Batchelor spectrum using highly resolved measurements of T and C in a laboratory flume. Measurements of T in the ocean by Dillon and Caldwell (1980) provided more support over much larger Reynolds numbers.

For temperature, the wavenumber transition between inertial–convective and viscous–convective subranges is defined by the constants C_θ and q in Eqs. (5) and (10), respectively, as $k_* = (C_\theta/q)^{3/2} \text{Pr}^{-1/2} k_b^T$, where the Prandtl number is $\text{Pr} \equiv \nu/D_T$. For $q = 3.7$ and $C_\theta = 0.4$, the transition wavenumber is $k_* = 0.014k_b^T$.

In seawater, salt fluctuations are diffused at scales 10 times smaller than temperature fluctuations because of the large Schmidt number. Consequently, the salinity gradient spectrum peaks at wavenumbers $\sqrt{\text{Sc}} \sim 10$ times higher than the temperature gradient spectrum.

3. Theoretical conductivity spectra

Conductivity is a function of both S and T and may be linearized near C_o :

$$C(T, S) = C_o + aS + bT \quad \begin{cases} a = \left. \frac{\partial C}{\partial S} \right|_{C_o} \\ b = \left. \frac{\partial C}{\partial T} \right|_{C_o} \end{cases} \quad (11)$$

For seawater at 35 psu and 10°C, $a \sim 0.092 \text{ S m}^{-1} \text{ psu}^{-1}$ and $b \sim 0.090 \text{ S m}^{-1} \text{ K}^{-1}$. This indicates that a 1-K change in T has about the same effect on C as a 1 psu change in S . This range in ΔT and ΔS is typical of our data. The vertical gradient in conductivity ($\partial C/\partial z$) may be expressed in terms of the salinity and temperature gradients ($\partial S/\partial z$, $\partial T/\partial z$):

$$\frac{\partial C}{\partial z}(T, S) = a \frac{\partial S}{\partial z} + b \frac{\partial T}{\partial z}. \quad (12)$$

The conductivity gradient spectrum $\Psi_{C_z}(k)$ is then related to the temperature $\Psi_{T_z}(k)$ and salinity $\Psi_{S_z}(k)$ gradient spectra by (see Washburn et al. 1996)

$$\Psi_{C_z}(k) = a^2 \Psi_{S_z}(k) + 2ab \Psi_{T_z S_z}(k) + b^2 \Psi_{T_z}(k), \quad (13)$$

where $\Psi_{T_z S_z}(k)$ represents the temperature–salinity gradient cross spectrum.

The gradient autospectra $\Psi_{T_z}(k)$ and $\Psi_{S_z}(k)$ are positive and real by definition. The cross-spectral term is complex in general and may be written as

$$\Psi_{T_z S_z}(k) = \gamma_{S_z T_z}(k) e^{i\phi(k)} \sqrt{\Psi_{T_z}(k) \Psi_{S_z}(k)}, \quad (14)$$

where $\gamma_{S_z T_z}(k)$ is the coherence and $\phi(k)$ is the phase between S_z and T_z at wavenumber k .

Pure mixing of two water masses with distinct T and S produces a linear T – S relation. Hence, fluctuations in T are highly correlated with fluctuations in S in the inertial subrange. The influence of molecular diffusion should become important only at higher wavenumbers. Near k_b^T we should expect low coherence between T_z and S_z because of the differences in D_T and D_S (thermal gradients are smeared by molecular diffusion at scales where salinity gradients remain intact).

When $\gamma_{S_z T_z}(k)$ is significant, $\phi(k)$ is determined by the T – S relation of the large-eddy scales. For $k < k_b^T$, a high coherence [near $\gamma_{S_z T_z}(k) \sim 1$] is expected because the differences in scalar diffusivities should not be important. The phase should be near $\phi \sim 0$ or $\phi \sim \pi$, depending on the sign of the slope of the T – S relation. For $\phi = 0$, positive fluctuations in T correspond to positive fluctuations in S , while when $\phi = \pi$, positive fluctuations in T correspond to negative fluctuations in S .

The large-scale T – S characteristics of a turbulent patch determine whether the cross spectrum tends to enhance or nullify the spectrum of conductivity. To illustrate these effects, synthetically generated conductivity datasets were created by inverse Fourier transforming Batchelor spectra into spatial records for T and

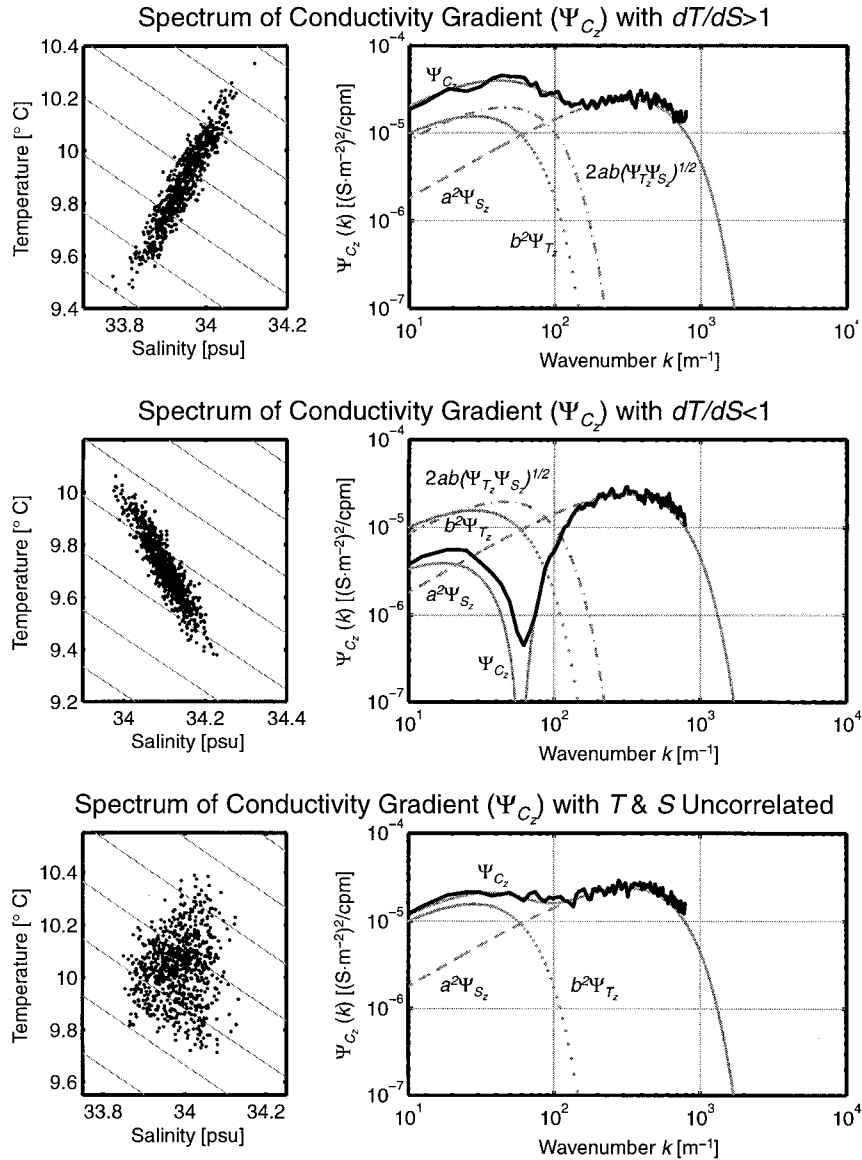


FIG. 2. Conductivity spectra for three synthetically generated patches having identical χ_T and χ_S but differently correlated T - S relations (for each patch, $\epsilon = 10^{-8} \text{ m}^2 \text{ s}^{-3}$, $\chi_T = 10^{-7} \text{ K}^2 \text{ s}^{-1}$, and $\chi_S = 10^{-8} \text{ psu}^2 \text{ s}^{-1}$). The solid gray curve is the expected conductivity spectrum for the given T - S characteristics. The black curve is the conductivity spectrum of the synthetically generated data. The individual contributions from $a^2\Psi_{S_z}$, $b^2\Psi_{T_z}$, and $2ab\sqrt{\Psi_{T_z}\Psi_{S_z}}$ are represented by the dotted, dashed, and dash-dotted curves, respectively. When T and S are positively correlated, $\Psi_{S_z T_z}$ has a positive contribution to Ψ_{C_z} (top). If T and S are negatively correlated, $\Psi_{S_z T_z}$ removes variance from Ψ_{C_z} (middle). When T and S are uncorrelated, the cross spectrum is zero (bottom).

S . Figure 2 shows three T - S relations and their effect on conductivity spectra. The different T - S properties were obtained by constraining the phase between T and S to be 0, π , or random. Here, C was derived from the T and S series, and its spectrum calculated. In all three cases, the dotted ($b^2\Psi_{T_z}$), dashed ($a^2\Psi_{S_z}$), and dash-dotted ($2ab\sqrt{\Psi_{T_z}\Psi_{S_z}}$) curves are identical. (Note that the dash-dot curve is not shown in the last case since

it does not contribute to Ψ_{C_z} , as described below.) Differences in conductivity spectra arise solely from the value of ϕ . In the top plot, T and S are positively correlated ($\gamma_{S_z T_z} = 1$, $\phi = 0$) at all wavenumbers, and the conductivity spectrum is the sum of all three spectra. In the middle plot, T and S are negatively correlated ($\gamma_{S_z T_z} = 1$, $\phi = \pi$), so that the conductivity spectrum is the sum of the temperature and salinity spectra minus

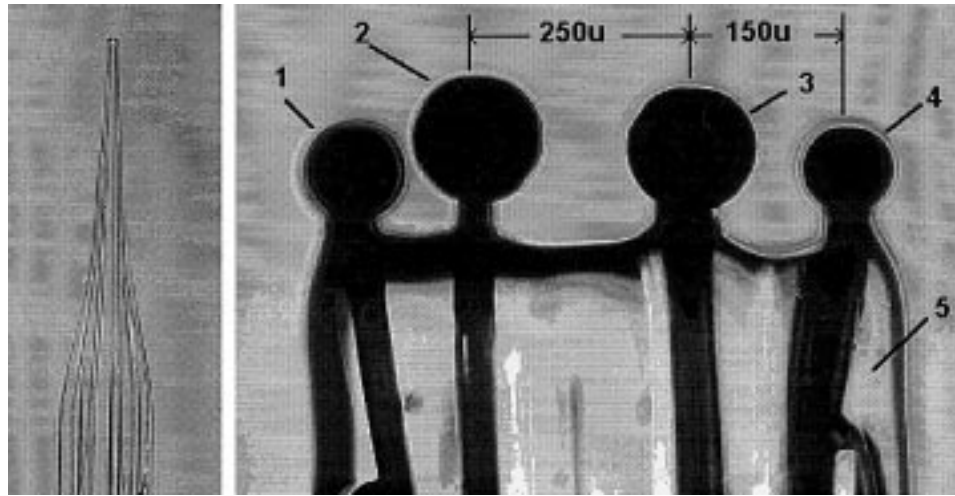


FIG. 3. The upper inch of the fast-response conductivity probe (left; magnification 5 \times) is shown along with a magnified (200 \times) cross section of the tip (right). The probe was constructed by M. Head at Precision Measurement Engineering and consists of two current-supplying (2, 3) and two voltage-measuring spherical platinum electrodes (1, 4) supported by a fused glass matrix (5). The sensor averages conductivity over a bipolar volume of radial extent ~ 3 mm and has a -3 -dB power attenuation near $k \sim 300$ cpm (photographs courtesy of M. Head).

the T - S cross spectrum. When T and S are uncorrelated (bottom plot), there is no cross-spectral contribution ($\gamma_{S_z T_z} = 0$) and the conductivity spectrum is the sum of the temperature and salinity spectra alone.

To predict the shape of the conductivity spectrum, it is necessary to estimate the relative magnitudes of χ_T and χ_S . One means of estimating χ_S is from χ_T and the mean gradients in T and S (Gregg 1984, 1987; Gargett and Moum 1995). If it is assumed that fluctuations in

T and S are produced by turbulent overturns, then the ratio of fluctuations should be proportional to the gradient T - S relation at the scale of the overturn, and it follows from Eqs. (1) and (6) that

$$\chi_S = \left(\frac{dS}{dT} \right)^2 \chi_T. \quad (15)$$

Note that dimensional analysis suggests that Ψ_{θ_z} be pro-

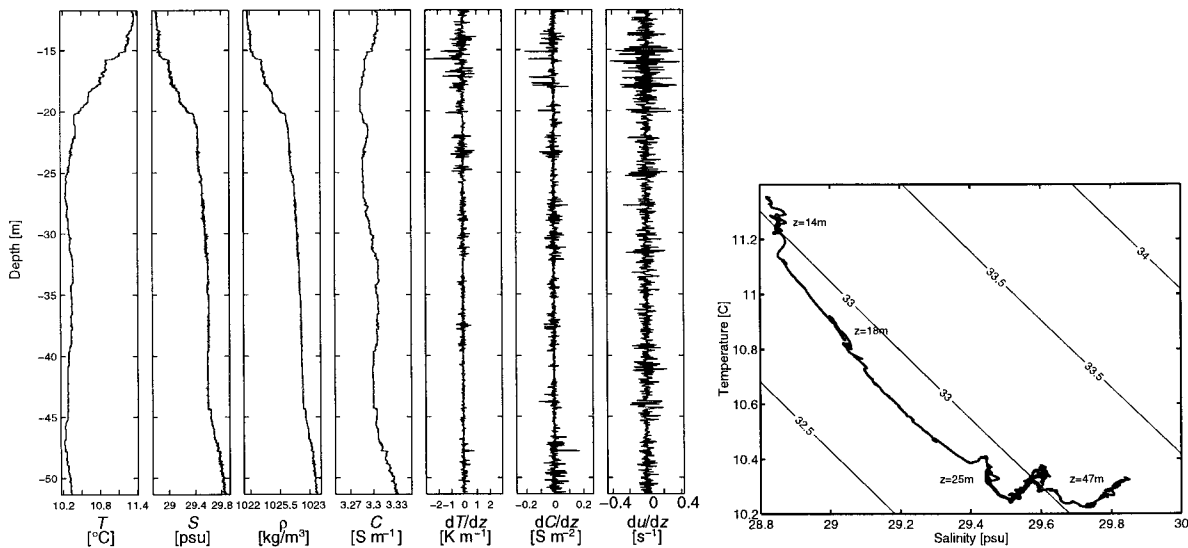


FIG. 4. Vertical profiles and $T - S$ relation for the Haro Strait drop 1685. Here, T , S , and C have each been scaled so that “full scale” represents a change in conductivity of approximately 0.1 S m^{-1} . The term dT/dz is also scaled with respect to dC/dz (full scale represents $\sim 0.25 \text{ S m}^{-2}$). All signals have been low-pass filtered at 10 cm. Lines of constant conductivity are shown in gray in the T - S diagram.

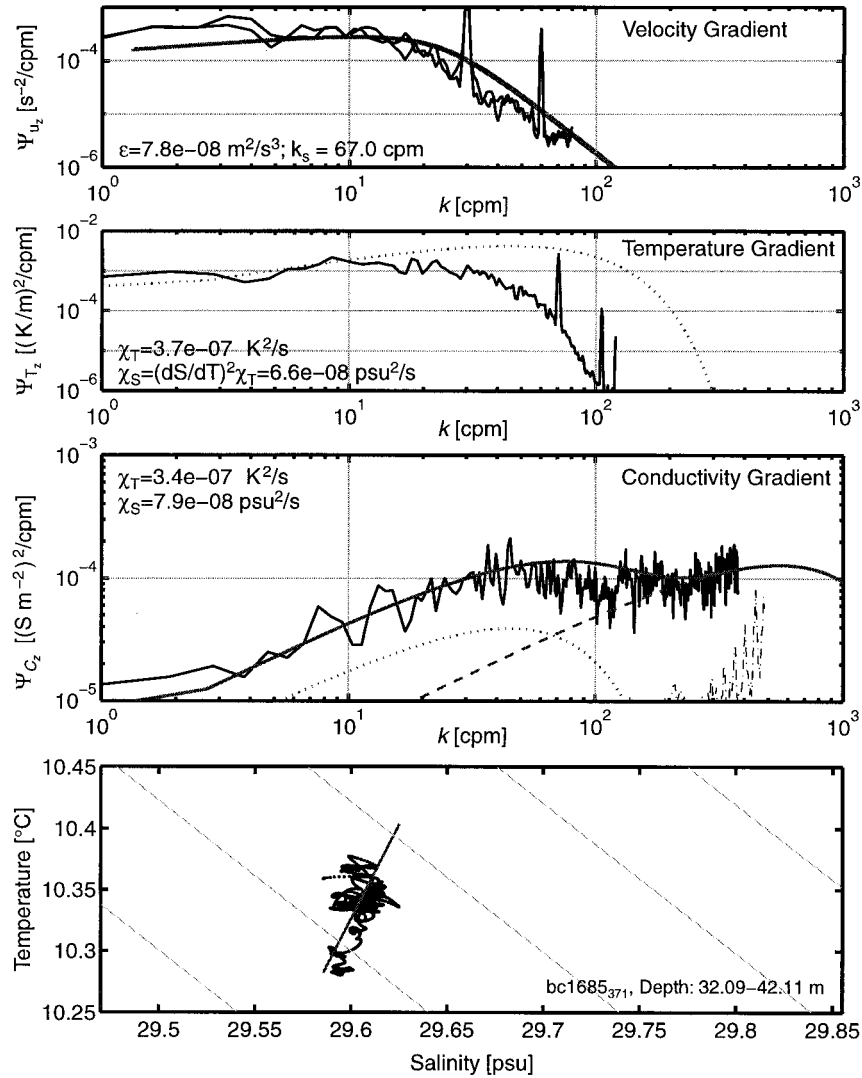


FIG. 5. Spectra of velocity shear, temperature gradient, and conductivity gradient for a patch in which the temperature contribution dominates Ψ_{C_z} , having $dS/dT = 0.4$ psu K^{-1} . The top plot shows spectra from the two shear probes and the corresponding Nasmyth spectra used for integration correction in the estimate of ϵ , k_s , and k_b^+ . The spikes at 30 and 60 cpm are the result of contamination from an electromagnetic velocity sensor and do not affect the estimate of ϵ or k_b^+ . The second plot shows Ψ_{T_z} from the FP07 thermistor (solid line) and the Batchelor spectral shape using k_b calculated from Ψ_{u_z} and the same integrated variance as the thermistor data below 10 cpm [see Eq. (16)]. Corrections have not been applied to the FP07 spectrum, because of uncertainties in the sensor's frequency response (Nash et al. 1998, manuscript submitted to *J. Atmos. Oceanic Technol.*). In the third plot, the thick gray curve represents $[\Psi_{C_z}]_{\text{theory}}$, which has contributions from Batchelor spectra for temperature (dotted line), salinity (dashed line), and the T - S cross spectrum (not shown). The thin dashed line shows a typical noise spectrum for the probe. The term dS/dT was obtained from the slope of the T - S diagram (gray line, bottom plot), k_b^+ was calculated from Ψ_{u_z} , and χ_T determined by satisfying Eq. (16) over the range $0 < k < 0.2k_b^+$. The estimates of χ_T and χ_S from both Ψ_{T_z} and Ψ_{C_z} are shown on the plots and are remarkably consistent.

portional to χ_θ at low wavenumbers. Thus, even if the Batchelor spectral shape is not the appropriate form, the relative sizes of χ_T and χ_S should be indicative of the magnitudes of Ψ_{T_z} and Ψ_{S_z} .

4. Experimental data

A conductivity probe capable of resolving high wavenumbers is shown in Fig. 3, and its spatial response is

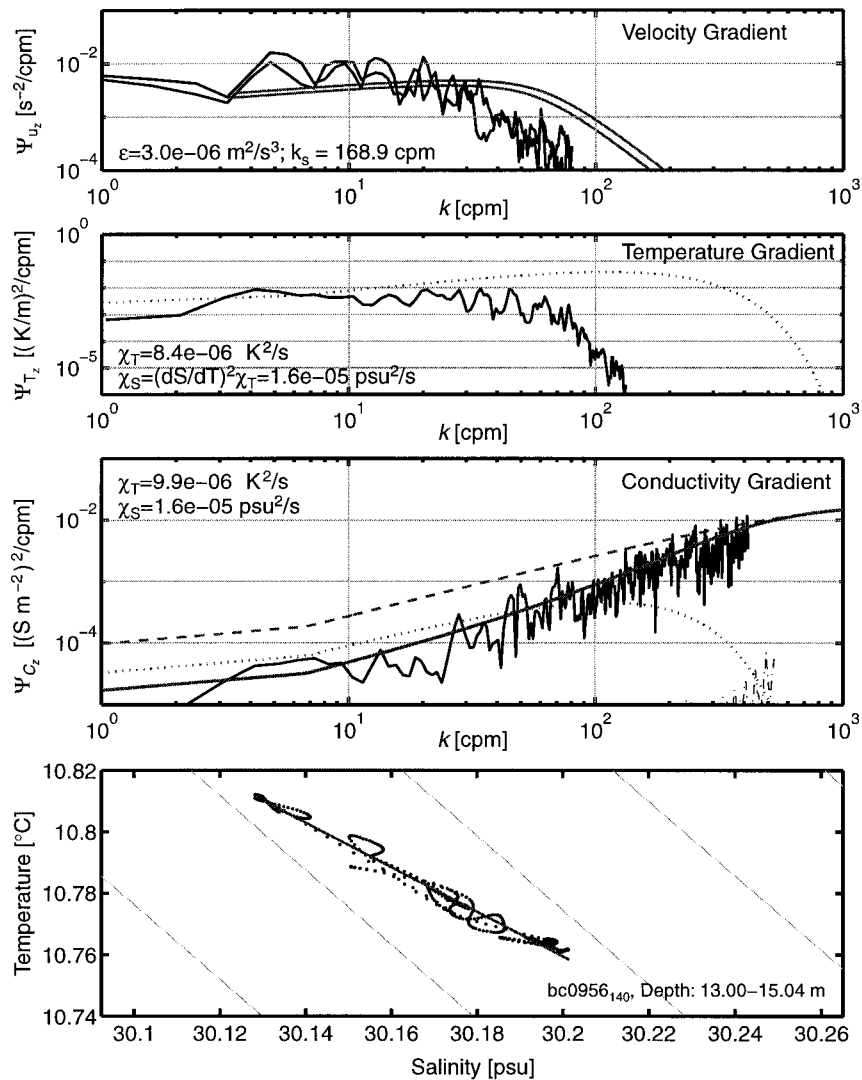


FIG. 6. Spectra of velocity shear, temperature gradient, and conductivity gradient for a patch with $dS/dT = -1.4$ psu K^{-1} (see Fig. 5 for description). Because the large-scale $T-S$ structure is nearly aligned along lines of constant conductivity, the conductivity spectrum (solid gray line) at low wavenumbers is less than the individual contributions of either temperature (dotted line) or salinity (dashed line). Regardless, the estimates of χ_T and χ_S made independently from Ψ_{T_z} and Ψ_{C_z} agree remarkably well.

described in detail in the appendix. This probe has been used on our vertical microstructure profiler *Chameleon* during experiments in the northeast Pacific Ocean (~1000 miles off Northern California) (Moum 1996) and in Haro Strait (Gargett and Moum 1995), a tidal channel in British Columbia, Canada. Between these two experiments, a wide variety of $T-S$ characteristics were encountered as well as a large range in ϵ , χ_T , and χ_S .

A cluster of microstructure sensors including two air-foil shear probes (used to estimate ϵ) (e.g., Moum et al. 1995), a Neil Brown conductivity cell (used for fast-conductivity calibration), and a fast-response FP07

thermistor accompanied the fast four-point conductivity probe.

A typical profile from these measurements and a $T-S$ diagram from Haro Strait are shown in Fig. 4. The $T-S$ characteristics of this region exhibit a wide range in dS/dT , which is a measure of whether the conductivity signal is temperature or salinity dominated. This, in turn, yields a large range of χ_S/χ_T [as a result of Eq. (15)], which is the important parameter in describing the shape of $\Psi_{C_z}(k)$.

The influence of T and S on the conductivity signal may be seen in these properly scaled vertical profiles. Where the mean vertical gradients in T and S are of

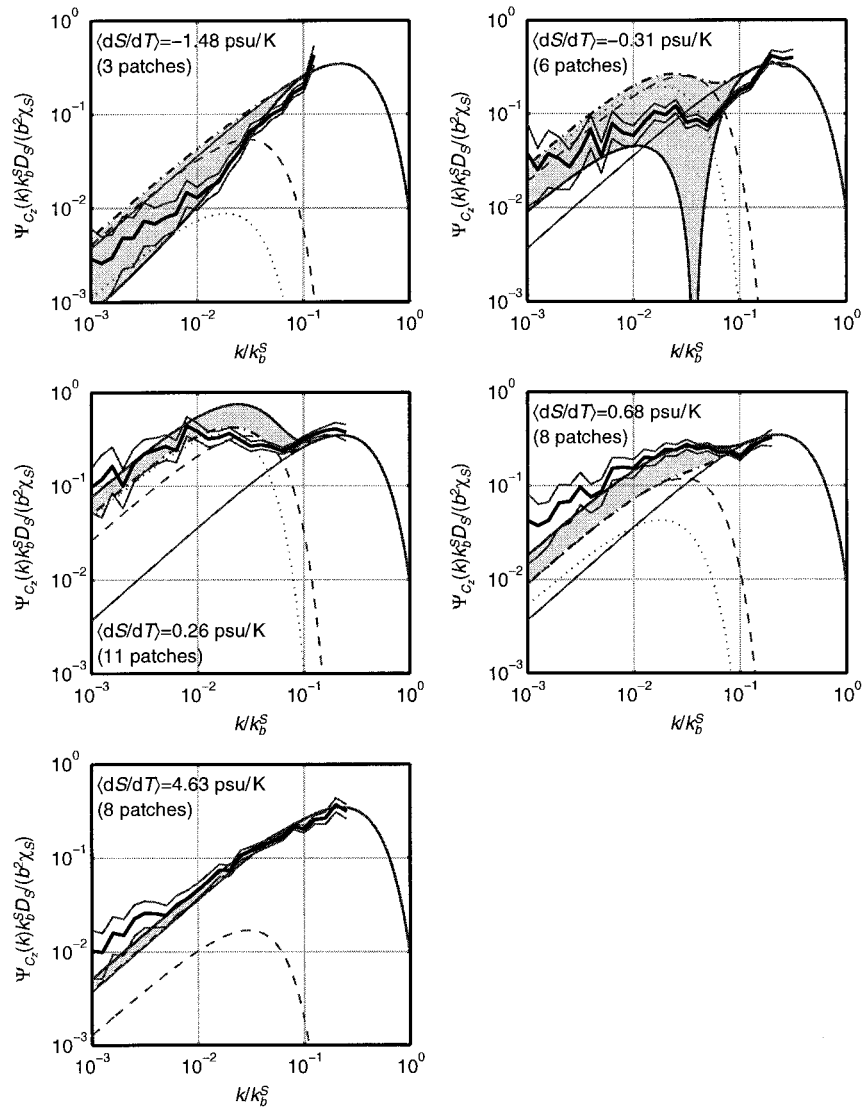


FIG. 7. Nondimensional conductivity gradient spectra for five ranges of dS/dT . Spectral values are nondimensionalized with respect to salinity as $\Psi_{c_i} k_b^S D_s b^{-2} \chi_s^{-1}$ and to wavenumber as k/k_b^S . In each case, the mean $\langle dS/dT \rangle$ was calculated for each group of patches and used to estimate the magnitude of χ_T/χ_S . The spectral amplitudes are normalized by $b^2 \chi_S (k_b^S D_s)^{-1}$, and wavenumber by k_b^S . The thick solid gray line shows the expected Ψ_{c_i} if T and S are perfectly correlated at all wavenumbers. The dash-dotted line indicates the spectrum for uncorrelated T and S . The shaded area is the region $0 < \gamma_{S, T_z} < 1$. The dotted, dashed, and thin solid lines represent the contributions from Ψ_{T_z} , Ψ_{S, T_z} , and Ψ_{S_c} , respectively.

opposite sign ($\sim 15\text{--}20$ m), changes in T and S have opposing influences on C , and hence, the dT/dz signal is larger than dC/dz . On a T - S diagram, this is represented by a line sloping from upper left to lower right. Large dC/dz signal (relative to dT/dz) occurs where positive changes in T correspond to positive changes in S ($\sim 30\text{--}34$ m and $\sim 47\text{--}51$ m, for example) because those T - S changes both produce a rise in C (T - S is aligned nearly perpendicular to the first case).

Patches were selected for homogeneity in ϵ and χ_T ,

so that cutoff wavenumbers k_b^T and k_b^S and spectral amplitudes Ψ_{U_s} and Ψ_{T_z} are well defined. Patches with low turbulent kinetic energy (TKE) dissipation rates, $\epsilon < 5 \times 10^{-6} \text{ m}^2 \text{ s}^{-3}$, were preferentially selected to resolve as close to $k \sim k_b^S$ as possible. Furthermore, a well-defined and linear T - S relation was required in order to make comparisons between χ_S and χ_T possible [i.e., permitting the basic assumption leading to Eq. (15)] and to help ensure homogeneity of the salinity fluctuations.

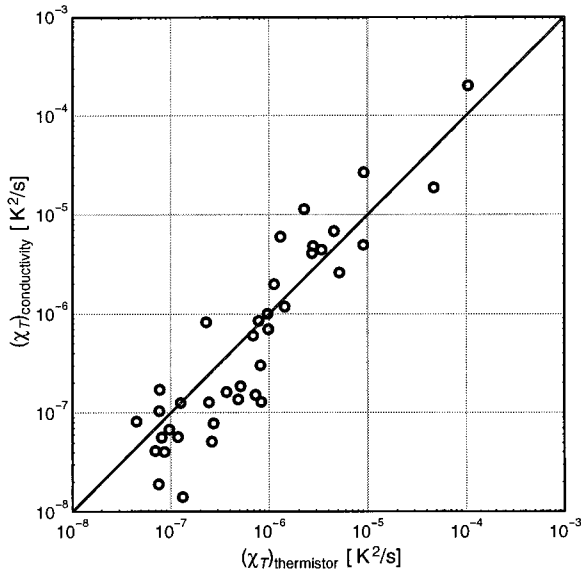


FIG. 8. Dissipation rate of temperature variance calculated from conductivity is compared to thermistor measurements.

5. Calculating χ_θ from scalar gradient spectra

In principle, scalar dissipation rates can be calculated by directly integrating the scalar gradient spectrum [Eq. (6)]. In practice, microstructure measurements are seldom resolved at the highest wavenumbers due to limitations of sensor response. As a result, scalar gradient spectra can be integrated only over a subrange from $k_{\min}^\theta < k < k_{\max}^\theta$, where generally $k_{\min}^\theta = 0$. To account for variance not resolved by the probe, we assume the theoretical gradient spectrum $[\Psi_{\theta_z}(k)]_{\text{theory}}$ of Batchelor [Eq. (10)]. Using k_b^θ from Eq. (8) and ϵ from two independent shear probe estimates, the only unknown in this equation is χ_θ , which can be determined by requiring

$$\int_{k_{\min}^\theta}^{k_{\max}^\theta} [\Psi_{\theta_z}(k)]_{\text{probe}} dk = \int_{k_{\min}^\theta}^{k_{\max}^\theta} [\Psi_{\theta_z}(k)]_{\text{theory}} dk, \quad (16)$$

where $[\Psi_{\theta_z}(k)]_{\text{probe}}$ is the gradient spectrum as measured by the probe.

The choice of k_{\max}^θ depends on the sensor. For example, the response of our FP07 thermistor is attenuated at frequencies above approximately 10 Hz (Lueck et al. 1977). Since there can be considerable uncertainty in the probe response corrections (Nash et al. 1998, manuscript submitted to *J. Atmos. Oceanic Technol.*), we used $k_{\min}^T = 0$, $k_{\max}^T = (7 \text{ Hz})/U_o \sim 10 \text{ cpm}$ (where U_o is the instrument's fall speed) to make conservative estimates of χ_T .

The spatial response of the conductivity probe in Fig. 3 is described in the appendix and has a half-power point at 300 cpm. Due to a lack of understanding of the probe response at the time of the experiments, the probe was not sampled fast enough (or it profiled too

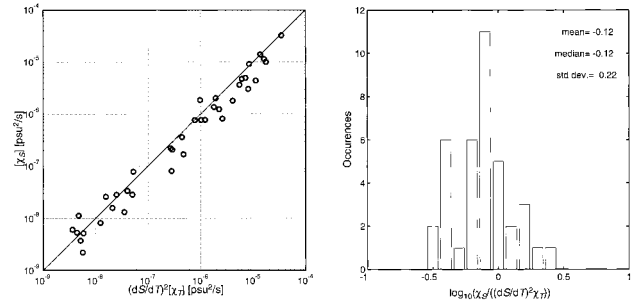


FIG. 9. Salinity variance dissipation rate compared to $(dS/dT)^2 \chi_T$. The histogram indicates that χ_S is on average about 25% less than $(dS/dT)^2 \chi_T$. The significance of this deviation is not clear.

quickly) to resolve its full spatial potential. Instead it was antialias filtered at 320 Hz and sampled at 819.2 Hz. Corrections for the filter and sensor's spatial response were applied so that the Nyquist frequency ($f_N = 409.6 \text{ Hz}$) limits the response at $k_{\max}^\theta = (409.6 \text{ Hz})/U_o \sim 500 \text{ cpm}$.

Estimating χ_T and χ_S from conductivity measurements using Eq. (16) is simplified by writing the composite spectrum $[\Psi_{C_z}]_{\text{theory}}$ as the sum of three Batchelor spectra [Eq. (13)]. This is accomplished by relating χ_S to χ_T using Eq. (15) and dS/dT over the patch; k_b^T and k_b^S depend primarily on ϵ , as determined from the airfoil probes. For perfect coherence and phase ($\gamma_{S_z T_z} = 1$ and $e^{i\phi} = \pm 1$) at all wavenumbers, $[\Psi_{C_z}(k)]_{\text{theory}}$ can be written in terms of either χ_T or χ_S using Eqs. (13) and (14) and assuming the Batchelor spectral form [Eq. (10)] for $[\Psi_{T_z}(k)]_{\text{theory}}$ and $[\Psi_{S_z}(k)]_{\text{theory}}$.

Estimation of χ_T from the conductivity sensor is accomplished by satisfying Eq. (16) with Ψ_{C_z} expressed in terms of χ_T . By selecting $k_{\min}^C = 0$ and $k_{\max}^C = 0.2k_b^T$, we integrate Ψ_{C_z} over a region where we are confident that the coherence between T and S is near unity, and thus, our estimate of $\Psi_{S_z T_z} = \pm \sqrt{\Psi_{T_z} \Psi_{S_z}}$ is justified. Since $\Psi_{T_z}(k)$ is not resolved for $k \gtrsim 0.2k_b^T$, it is not possible to estimate $\gamma_{S_z T_z}(k)$ near $k \sim k_b^T$. However, the assumption of $\gamma_{S_z T_z}(k) = 1$ must break down at high wavenumbers because of seawater's large Schmidt number. It is thus appropriate to choose k_{\max}^C conservatively in order to avoid integrating $\Psi_{C_z}(k)$ over a region in which $\Psi_{S_z T_z}(k)$ is unknown since a reliable estimation of χ_T can be made by integrating about 30% of the variance of $[\Psi_{T_z}(k)]_{\text{theory}}$, which is a consequence of this choice of k_{\max}^C .

Estimation of χ_S may be made by integrating Eq. (16) from $k_{\min}^C = 0.6k_b^T$ to $k_{\max}^C = f_N/U_o$. Since 90% of the variance in $[\Psi_{T_z}(k)]_{\text{theory}}$ occurs at wavenumbers below $0.6k_b^T$, this choice for k_{\min}^C ensures that Ψ_{C_z} is integrated over a bandwidth in which the contribution from T (i.e., $b^2 \Psi_{T_z}$) is minimal.

6. Sample spectra

Spectra of shear, temperature gradient, and conductivity gradient for two patches are shown in Figs. 5 and

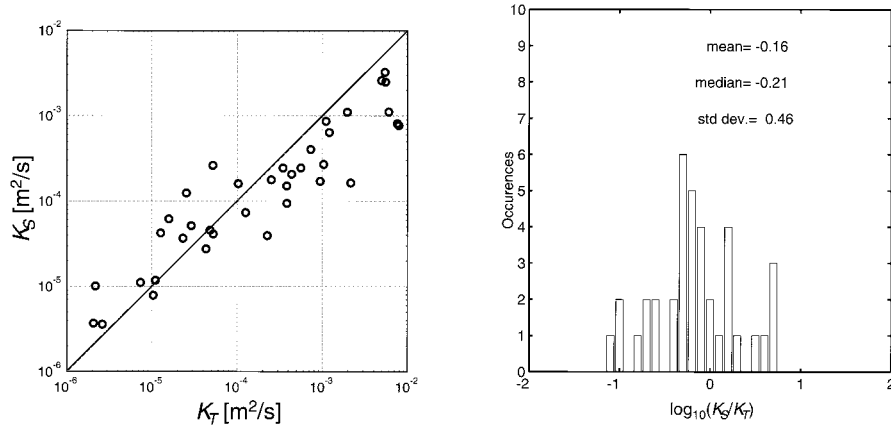


FIG. 10. Comparison of eddy diffusivities for heat and salt.

6. These examples illustrate two extremes in the shape of Ψ_{C_z} that result from the unique T - S characteristics of each patch.

The spectra in Fig. 5 correspond to the turbulent patch from 34.2 to 40.7 m for drop 1685 (see Fig. 4). In this case, T and S are positively correlated with $dS/dT = 0.4 \text{ psu K}^{-1}$. Since $dS/dT > 0$, the $\Psi_{S_z T_z}$ cross-spectral term makes a positive contribution to Ψ_{C_z} . In addition, the relatively low magnitude of dS/dT implies that the contribution from $b^2\Psi_{T_z}$ is much larger than $a^2\Psi_{S_z}$ at low wavenumbers. Consequently, the temperature roll-off near $k \sim k_b^T$ is evident in Ψ_{C_z} . The estimate of χ_T made from the conductivity probe ($3.4 \times 10^{-7} \text{ K}^2 \text{ s}^{-1}$) agrees well with that from the thermistor probe ($3.7 \times 10^{-7} \text{ K}^2 \text{ s}^{-1}$). Similarly, the estimate of χ_S made using Eq. (16) at high wavenumbers ($7.9 \times 10^{-8} \text{ psu K}^{-1}$) is consistent with $(dS/dT)^2\chi_T = 6.6 \times 10^{-8} \text{ psu K}^{-1}$, as predicted by Eq. (15).

Figure 6 presents spectra from a patch having $dS/dT = -1.4 \text{ psu K}^{-1}$. Under these circumstances, the contribution to Ψ_{C_z} from salinity dominates that from temperature at all wavenumbers. Further, fluctuations in T are negatively correlated with S and negate fluctuations in C so that $\gamma_{S_z T_z} \sim -1$. From Eq. (14), the cross spectrum is negative ($\Psi_{S_z T_z} < 0$), so that the second term in Eq. (13) reduces the amplitude of Ψ_{C_z} . The resulting conductivity spectrum Ψ_{C_z} in this case is less than the contribution from either temperature ($b^2\Psi_{T_z}$) or salinity ($a^2\Psi_{S_z}$) except at very high wavenumbers where the effects from fluctuations in T are minimal. In light of the destructive interference between T and S creating much reduced spectral amplitudes, the estimates of χ_T and χ_S between conductivity and thermistor probes are remarkably consistent.

7. Results

Averaged nondimensional conductivity gradient spectra are shown in Fig. 7 for five different ranges of

dS/dT . In the first two plots, $\langle dS/dT \rangle < 0$, and thus, $\Psi_{S_z T_z}$ reduces the spectral amplitudes of Ψ_{C_z} . In the last three plots, $\langle dS/dT \rangle > 0$, so that Ψ_{C_z} is the sum of the three components. Note that salinity dominates the spectra for $|\langle dS/dT \rangle| > 1 \text{ psu K}^{-1}$ (first and last plots), while both scalars contribute to the shape for $|\langle dS/dT \rangle| < 1 \text{ psu K}^{-1}$.

In the plots with $\langle dS/dT \rangle = -0.31 \text{ psu K}^{-1}$ and $\langle dS/dT \rangle = 0.26 \text{ psu K}^{-1}$, both T and S play significant roles in determining the shape of Ψ_{C_z} . Since thermal diffusion becomes important for $k \geq 0.1k_b^T$, it is expected that T and S should become less coherent at these wavenumbers and $\Psi_{S_z T_z}$ should be reduced in magnitude. As a result, these two conductivity spectra deviate from the solid curve ($\gamma_{S_z T_z} = 1$) for $0.1 \leq k_b^T \leq 1$ ($0.01 \leq k/k_b^S \leq 0.1$ in Fig. 7, where $k_b^S = \text{Sc}^{1/2}k_b^T \sim 10k_b^T$). Unfortunately, the lack of spatially coincident measurements of T and C from these experiments [on scales of $\sim O((k_b^T)^{-1})$] does not give us enough information to independently determine $\Psi_{S_z T_z}$. Hence, the degree to which $\gamma_{S_z T_z}$ deviates from unity at high wavenumbers remains to be determined.

The temperature dissipation rate estimated using the conductivity probe (χ_T)_{conductivity} is compared to that measured using the thermistor (χ_T)_{thermistor} in Fig. 8 for 38 patches. The salinity dissipation rate calculated from conductivity spectra [through Eq. (16)] is compared to that estimated using Eq. (15) in Fig. 9. In both cases, conductivity-derived quantities are consistent with those estimated using the thermistor probe.

Estimates of K_S and K_T using χ_S and χ_T from conductivity measurements are shown in Fig. 10. These are preliminary estimates, and the reason for the deviation in the ratio K_S/K_T from 1 is not clear. This is the focus of ongoing experiments and analysis.

8. Summary

Conductivity spectra have been resolved to wavenumbers greater than k_b^T , where the contribution to the

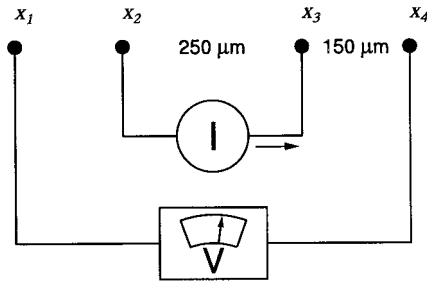


FIG. A1. Schematic of the four-point conductivity probe.

conductivity gradient spectrum is entirely due to salinity fluctuations. This has enabled direct estimates of χ_S to be made from Ψ_{C_z} at high wavenumbers. The term χ_T may be estimated from Ψ_{C_z} at lower wavenumbers as long as the contributions from $\Psi_{S_z T_z}$ and Ψ_{T_z} are accounted for. The magnitude and sign of $\Psi_{S_z T_z}$ can be estimated if the $T-S$ relation is well defined, and perfect coherence between T and S is assumed. This assumption of $\gamma_{S,T_z} = 1$ breaks down for $0.1k_b^T \lesssim k \lesssim 0.1k_b^S$, where the effects of thermal molecular diffusion become important to Ψ_{T_z} (but where the effects of salt diffusion by molecular processes are small). This is evident in the summary spectra of Fig. 7, where the data fall in the gray area of $0 < \gamma_{S,T_z} < 1$. We presume that the shape of $\Psi_{S_z T_z}$ is a function of the state of decay of the turbulence and that highly resolved, coincident measurements of T and C will be required to elucidate this.

We emphasize that the comparisons of χ_S versus $(dS/dT)^2 \chi_T$ are subject to two important constraints. The first is discussed in the preceding paragraph: $\gamma_{S,T_z} = 1$. In fact, the data have been chosen to avoid patches for which γ_{S,T_z} is clearly different than 1 (i.e., scatter in the $T-S$ relation). But since the smallest scales of $\Psi_{S_z T_z}$ are not resolved, we really do not know the true value of γ_{S,T_z} . This limits our ability to assign confidence to the estimates of χ_S and χ_T based on the integration of Ψ_{C_z} and motivates further experiments to resolve $\Psi_{S_z T_z}$ over the full wavenumber range. Such measurements will provide experimental tests of the relationships among tracer variance dissipations, as posed by de Szoeke (1998).

The second constraint is the assumption leading to Eq. (15). Again, the data have been chosen to select for linear $T-S$ in each sample. The reason for the deviation of the ratio $\chi_S [(dS/dT)^2 \chi_T]^{-1}$ is unknown at present but needs to be further examined before we make routine estimates of χ_S from Ψ_{C_z} .

Acknowledgments. We appreciate informative discussions with Jeff Dairiki, Doug Caldwell, and Roland de Szoeke. Our measurements would not have been possible without the skilled work of Mike Neeley-Brown, Mike Head, Ray Kreth, and Ed Llewelyn. This work was funded by the Office of Naval Research (N0014-

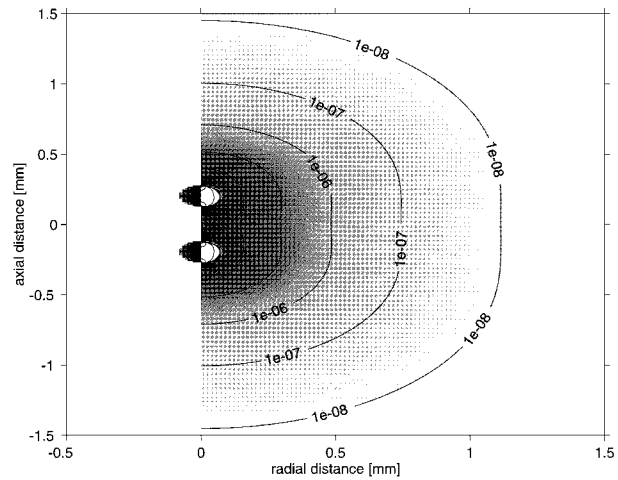


FIG. A2. Spatial sensitivity of the four-point conductivity probe. The sensitivity is radially symmetric about the y axis.

96-1-0250) and the National Science Foundation (OCE-9417018).

APPENDIX

Spatial Response of the Four-Point Conductivity Probe

Following Dairiki (1991), we approximate the conductivity probe shown in Fig. 3 as four single-point conductors having cylindrical symmetry, as schematized in Fig. A1. Hence, the effect of the glass support and the finite diameter spherical conductors are ignored. We wish to determine the sensitivity of the voltage V

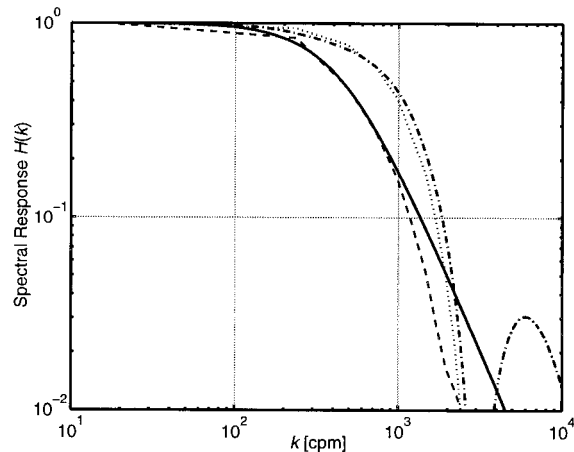


FIG. A3. Spatial transfer function for the conductivity probe. The dash-dotted line represents the 1D Fourier transform (with respect to x) of the spatial response function plotted in Fig. A2. The transfer function calculated by Head (1983) for a similar type probe is represented by the dotted line. The dashed line represents the experimentally observed sensitivity. Because of the similarity between theoretical (dotted and dash-dotted) curves, a double-pole filter (solid line) that approximates Head's measured transfer function was used for the spatial response correction.

measured between points \mathbf{x}_1 and \mathbf{x}_4 to small perturbations in the conducting medium when a constant current I flows between x_2 and x_3 . In a uniform medium of conductivity σ_o , the measured voltage V_o is simply

$$V_o = \frac{1}{4\pi\sigma_o} \left(\frac{1}{|\mathbf{x}_4 - \mathbf{x}_3|} + \frac{1}{|\mathbf{x}_2 - \mathbf{x}_1|} - \frac{1}{|\mathbf{x}_4 - \mathbf{x}_2|} - \frac{1}{|\mathbf{x}_3 - \mathbf{x}_1|} \right). \quad (\text{A1})$$

However, if the conductivity of the medium is given by

$$\sigma(\mathbf{x}) = \sigma_o + \sigma'(\mathbf{x}), \quad (\text{A2})$$

where $\sigma'(x)$ is the perturbation conductivity, then the measured voltage is obtained by a Green's solution:

$$V = V_o - \iiint_{\infty} \sigma'(\mathbf{x}) S(\mathbf{x}) d^3\mathbf{x}, \quad (\text{A3})$$

where $S(x)$ is the spatial sensitivity of the probe and d^3x represents a three-dimensional volume element. The sensitivity is

$$S(\mathbf{x}) = \frac{1}{16\pi^2\sigma_o^2} \left\{ \left(\frac{\mathbf{x}_3 - \mathbf{x}}{|\mathbf{x}_3 - \mathbf{x}|^3} - \frac{\mathbf{x}_2 - \mathbf{x}}{|\mathbf{x}_2 - \mathbf{x}|^3} \right) \times \left(\frac{\mathbf{x}_4 - \mathbf{x}}{|\mathbf{x}_4 - \mathbf{x}|^3} - \frac{\mathbf{x}_1 - \mathbf{x}}{|\mathbf{x}_1 - \mathbf{x}|^3} \right) \right\}. \quad (\text{A4})$$

A spectral transfer function may be defined as

$$H(k) = \left| \iiint_{\infty} S(x, y, z) e^{ikz} dx dy dz \right|^2, \quad (\text{A5})$$

where the measured spectral power from the sensor $\Psi_{\text{measured}}(k) = H(k)\Psi_{\text{real}}(k)$. For the probe locations sketched in Fig. A1, the radially symmetric spatial sensitivity is shown in Fig. A2. The one-dimensional transfer function of the probe was calculated by Fourier transforming the sensitivity and integrating over the transverse directions. The result of this calculation along with the transfer function of a similar probe as calculated by Head (1983) (but operated in a different configuration) is shown in Fig. A3. Head found that the experimentally observed resolution was somewhat lower than his calculated response, which is very similar to that calculated above. As a result, a double-pole filter response similar to that measured by Head (1983) was used as the transfer function for the current probe. This indicates that the 50% power point for the probe is near 300 cpm.

REFERENCES

- Batchelor, G. K., 1959: Small-scale variation of convected quantities like temperature in turbulent fluid. *J. Fluid Mech.*, **5**, 113–133.
- Corrsin, S., 1951: On the spectrum of isotropic temperature fluctuations in isotropic turbulence. *J. Appl. Phys.*, **22**, 469–473.
- Dairiki, G. T., 1991: Spatial response of a four-point conductivity probe. Report, University of Washington, 6 pp. [Available from School of Oceanography, University of Washington, Seattle, WA 98195-7940.]
- de Szoek, R. A., 1998: The dissipation of fluctuating tracer variances. *J. Phys. Oceanogr.*, **28**, 2064–2074.
- Dillon, T. M., and D. R. Caldwell, 1980: The Batchelor spectrum and dissipation in the upper ocean. *J. Geophys. Res.*, **85** (C4), 1910–1916.
- Gargett, A. E., 1985: Evolution of scalar spectra with the decay of turbulence in a stratified fluid. *J. Fluid Mech.*, **159**, 379–407.
- , and G. Holloway, 1992: Sensitivity of the GFDL ocean model to different diffusivities of heat and salt. *J. Phys. Oceanogr.*, **22**, 1158–1177.
- , and J. N. Moum, 1995: Mixing efficiencies in turbulent tidal fronts: Results from direct and indirect measurements of density flux. *J. Phys. Oceanogr.*, **25**, 2583–2608.
- Gibson, C. H., and W. H. Schwarz, 1963: The universal equilibrium spectra of turbulent velocity and scalar fields. *J. Fluid Mech.*, **16**, 365–384.
- Gregg, M. C., 1984: Entropy generation in the ocean by small-scale mixing. *J. Phys. Oceanogr.*, **14**, 688–711.
- , 1987: Diapycnal mixing in the thermocline: A review. *J. Geophys. Res.*, **92** (C5), 5249–5286.
- Head, M. J., 1983: The use of miniature four-electrode conductivity probes for high resolution measurement of turbulent density or temperature variations in salt-stratified water flows. Ph.D. thesis, University of California, San Diego, La Jolla, CA, 211 pp. [Available from Scripps Institution of Oceanography, UCSD, 9500 Gilman Dr., La Jolla, CA 92093.]
- Kraichnan, R., 1968: Small-scale structure of a scalar field convected by turbulence. *Phys. Fluids*, **11**, 945–953.
- Lueck, R. G., O. Hertzman, and T. R. Osborn, 1977: The spectral response of thermistors. *Deep-Sea Res.*, **24**, 951–970.
- Moum, J. N., 1996: Efficiency of mixing in the main thermocline. *J. Geophys. Res.*, **101** (C5), 12 057–12 069.
- , M. C. Gregg, R. C. Lien, and M. E. Carr, 1995: Comparison of turbulence kinetic energy dissipation rate estimates from two ocean microstructure profilers. *J. Atmos. Oceanic Technol.*, **12**, 346–366.
- Obukhov, A. M., 1949: The structure of the temperature field in a turbulent flow. *Izv. Akad. Nauk SSSR, Ser. Geogr. Geofiz.*, **13**, 58–69.
- Osborn, T. R., and C. S. Cox, 1972: Oceanic fine structure. *Geophys. Fluid Dyn.*, **3**, 321–345.
- Schmitt, R. W., 1979: Flux measurements on salt fingers at an interface. *J. Mar. Res.*, **37**, 419–436.
- , J. M. Toole, R. L. Koehler, E. C. Mellinger, and K. W. Doherty, 1988: The development of a fine- and microstructure profiler. *J. Atmos. Oceanic Technol.*, **5**, 484–500.
- Sreenivasan, K. R., 1996: The passive scalar spectrum and the Obukhov-Corrsin constant. *Phys. Fluids*, **8**, 189–196.
- Tennekes, H., and J. L. Lumley, 1972: *A First Course in Turbulence*. The MIT Press, 300 pp.
- Turner, J. S., 1965: The coupled turbulent transports of salt and heat across a sharp density interface. *Int. J. Heat Mass Transfer*, **8**, 759–767.
- Washburn, L., T. F. Duda, and D. C. Jacobs, 1996: Interpreting conductivity microstructure: Estimating the temperature variance dissipation rate. *J. Atmos. Oceanic Technol.*, **13**, 1166–1188.